Received: 23 February 2019 | Revised: 1 May 2019 | Accepted: 4 May 2019

DOI: 10.1002/acm2.12653

RADIATION ONCOLOGY PHYSICS

WILEY

Physical and biological impacts of collimator-scattered protons in spot-scanning proton therapy

Koki Ueno[1] | Taeko Matsuura[2,3,4] | Shusuke Hirayama[1,3] | Seishin Takao[3] | Hideaki Ueda[2] | Yuto Matsuo[3] | Takaaki Yoshimura[3] | Kikuo Umegaki[2,3,4]

[1]Graduate School of Biomedical Science and Engineering, Hokkaido University, Sapporo, Hokkaido, Japan

[2]Faculty of Engineering, Hokkaido University, Sapporo, Hokkaido, Japan

[3]Proton Beam Therapy Center, Hokkaido University Hospital, Sapporo, Hokkaido, Japan

[4]Global Station for Quantum Medical Science and Engineering, Global Institution for Collaborative Research and Education (GI-CoRE), Hokkaido University, Sapporo, Japan

Author to whom correspondence should be addressed. Taeko Matsuura
E-mail: matsuura@med.hokudai.ac.jp; Telephone: +81-11-706-5254; Fax: +81-11-706-5255.

Funding information
JSPS KAKENHI, Grant/Award Number: 18K07621; Ministry of Education, Culture, Sports, Science and Technology

Abstract

To improve the penumbra of low-energy beams used in spot-scanning proton therapy, various collimation systems have been proposed and used in clinics. In this paper, focused on patient-specific brass collimators, the collimator-scattered protons' physical and biological effects were investigated. The Geant4 Monte Carlo code was used to model the collimators mounted on the scanning nozzle of the Hokkaido University Hospital. A systematic survey was performed in water phantom with various-sized rectangular targets; range (5–20 cm), spread-out Bragg peak (SOBP) (5–10 cm), and field size (2×2–16×16 cm^2). It revealed that both the range and SOBP dependences of the physical dose increase had similar trends to passive scattering methods, that is, it increased largely with the range and slightly with the SOBP. The physical impact was maximized at the surface (3%–22% for the tested geometries) and decreased with depth. In contrast, the field size (FS) dependence differed from that observed in passive scattering: the increase was high for both small and large FSs. This may be attributed to the different phase-space shapes at the target boundary between the two dose delivery methods. Next, the biological impact was estimated based on the increase in dose-averaged linear energy transfer (LET_d) and relative biological effectiveness (*RBE*). The LET_d of the collimator-scattered protons were several keV/μm higher than that of unscattered ones; however, since this large increase was observed only at the positions receiving a small scattered dose, the overall LET_d increase was negligible. As a consequence, the *RBE* increase did not exceed 0.05. Finally, the effects on patient geometries were estimated by testing two patient plans, and a negligible *RBE* increase (0.9% at most in the critical organs at surface) was observed in both cases. Therefore, the impact of collimator-scattered protons is almost entirely attributed to the physical dose increase, while the *RBE* increase is negligible.

KEY WORDS
collimator scattering, linear energy transfer, pencil beam scanning proton therapy, relative biological effectiveness

This is an open access article under the terms of the Creative Commons Attribution License, which permits use, distribution and reproduction in any medium, provided the original work is properly cited.
© 2019 The Authors. *Journal of Applied Clinical Medical Physics* published by Wiley Periodicals, Inc. on behalf of American Association of Physicists in Medicine

1 | INTRODUCTION

Most newly built proton therapy centers worldwide are implementing the pencil beam scanning (PBS) technique because of its distinct advantages of dose conformity to targets and neutron exposure reduction compared to the more conventional passive scattering methods. However, when shallow tumors are involved, the large spot size of the low-energy proton beam resulting from the large-angle Coulomb scattering might offset the dose conformity advantage gained by the scanning approach.[1] To overcome this problem, different collimators have been designed and increasingly used in the clinics[2–4] and their clinical benefits have been investigated in various studies, with positive results.[5]

So far, most of the analytical dose calculation engines installed in the PBS treatment planning systems (TPSs) assume the collimator absorbs all the incident protons; that is, they neglect the dose contamination from the protons scattered by the collimator edge, while several studies have proven it could have a considerable dosimetric impact in reality. Van Luijk et al.[6] used a 160-MeV proton beam to measure and simulate scatter protons for a small field (<2 cm), showing that this contribution can be up to 20% at the patient surface. Titt et al.[7] conducted a systematic Monte Carlo study with various target sizes and depths used in the clinics; they also suggested there is contamination from scattered protons. However, both studies focused on the scattering approach and did not systematically investigate the collimators used in PBS.

Collimator-scattered protons can have an additional biological impact. The protons lose energy when hitting the collimator, and their linear energy transfer (LET) increases accordingly. A higher proton LET generates a greater biological effect, as observed in both *in vivo* and *in vitro* experiments[8–12] and even in the clinical outcome.[13] In the previously mentioned study, van Luijk et al.[6] estimated the increase of the biological damage based on a simple assumption that the protons with energy above 40 MeV have a relative biological effectiveness (RBE) of 1, while for those below 40 MeV have RBE of 1.2. In their experimental setup, only 5% of protons have the energy below 40 MeV at just below the collimator, implying that the biological damage to tissues would be at most 1% larger than that expected from the physical dose. Followed by the recent rapid progress of biophysical RBE models,[8,14] it may be interesting to revisit the biological impact of scattered protons.

In this study, we investigated the physical and biological impacts of the collimator-scattered protons used in the PBS system of the Hokkaido University Hospital. We systematically evaluated the effects of the collimator-scattered protons on the physical dose, the dose-averaged LET (LET_d), and the RBE. To evaluate the effects in real clinical settings, we simulated two patient plans. Finally, the difference between the PBS and passive scattering systems were discussed.

2 | MATERIALS AND METHODS

2.A | Beam collimation system for the spot-scanning beamline

The beam collimation system used for the spot-scanning beamline simulated in this study was an extrapolation of a short-range applicator (SRA) investigated by Yasui et al.[3] and consisted of a 2- or 4-cm thick brass collimator and a 4-cm thick energy absorber made of acrylonitrile–butadiene–styrene (ABS) plastic (Fig. 1). In the following paragraphs, it will be referred to simply as SRA. It was mounted at the most downstream portion of the gantry, with the lower surface of the collimator placed at 9 cm from the isocenter, and designed to have a maximum uniform field of 20 × 20 cm^2 at the isocenter. When using the configuration with the 2-cm thick collimator, the minimum and maximum available proton ranges after passing through a 4-cm thick energy absorber were 0.5 cm (74.9 MeV) and 10 cm (142.5 MeV) in water, respectively, and the in-air spot size at the isocenter ranged from 11.7 to 6.0 mm (one sigma). When using the 4-cm thick collimator, the minimum and maximum proton ranges were 0.5 cm (74.9 MeV) and 20 cm (192.4 MeV) in water, respectively, and the in-air spot size ranged from 11.7 to 5.3 mm (one sigma).

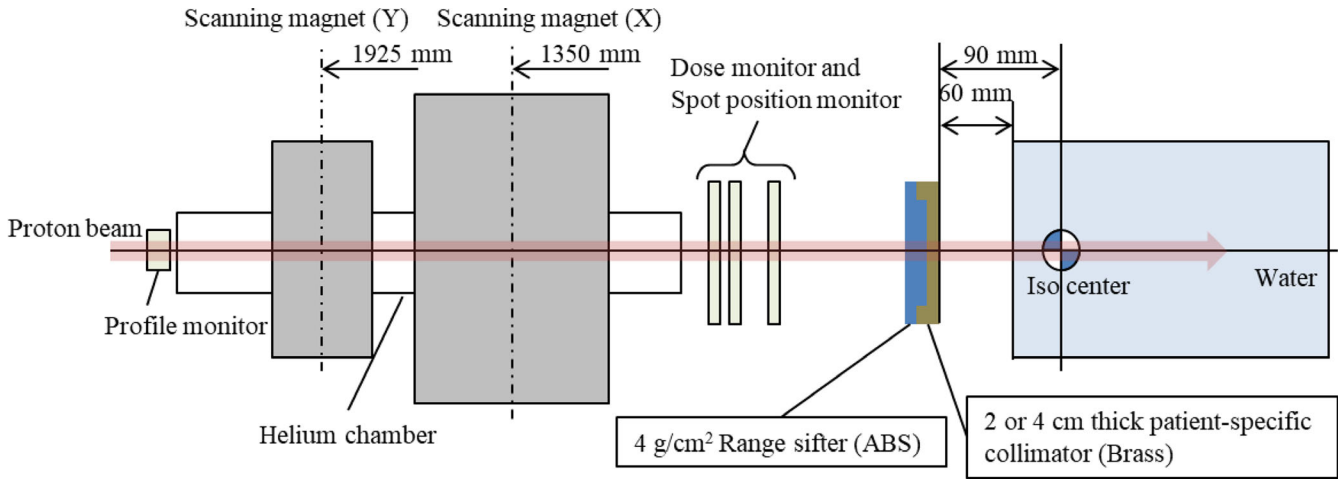

FIG. 1. Schematic representation of the treatment nozzle with the modeled beamline and water phantom. The range sifter was made of acrylonitrile–butadiene–styrene (ABS).

2.B | Simulations

2.B.1 | Monte Carlo code

The Geant4 Monte Carlo code (ver.4.10.p01)[15] was used together with the Particle-Therapy Simulation Framework (PTSim),[16] a wrapper of the Geant4 toolkit that facilitates particle-therapy simulation, to calculate the dose and LET_d distributions. The scanning nozzle of the Hokkaido University Proton Beam Therapy Centre and the SRA were modeled with different collimator opening shapes. The electromagnetic, hadron elastic and inelastic interactions were respectively simulated with the G4EmStandardPhysics option3, G4HadronElasticPhysics, and G4HadronPhysicsFTF BIC classes. The production threshold for all secondary particles was set to 1 mm. The initial beam parameters in the Monte Carlo code (i.e., Twiss parameters, emittance, mean energy, and energy dispersion) were selected to reproduce the integral depth dose and lateral beam profile in water for the nozzle with the energy absorber. Some of the validation results, up to the range of 10 cm, are illustrated in Fig. 2 and the supplementary material. In the Monte Carlo simulation, the number of protons per field was changed from 0.5×10^8 to 20×10^8 and their distribution in each spot depended on their intensity. The voxel size was set to $1 \times 1 \times 1$ mm^3.

2.B.2 | Target geometry

To systematically investigate the physical dose and *RBE* increase caused by the collimator-scattered protons, the simulation was performed for different target geometries in a water tank, and their parameters are summarized in Table 1 with the corresponding abbreviations. For the target maximum range below and above 10 cm, the SRA with the 2- and the 4-cm thick collimator respectively was used for the simulation. Below, we refer R[L_1]_S[L_2]_FS[L_3] to the target with range of L_1 [cm], SOBP width of L_2 [cm], and FS of $L_3 \times L_3$ [cm^2]. The water surface was set 6 cm downstream of the collimator with the isocenter located at 3 cm depth in water (Fig. 1). The

TABLE 1 Target geometry parameters used for the simulation

Range (R) [cm]	5, 10, 15, 20
spread-out Bragg- peak (SOBP) (S) [cm]	5, 10
Field size (FS) [cm^2]	2×2, 4×4, 8×8, 16×16

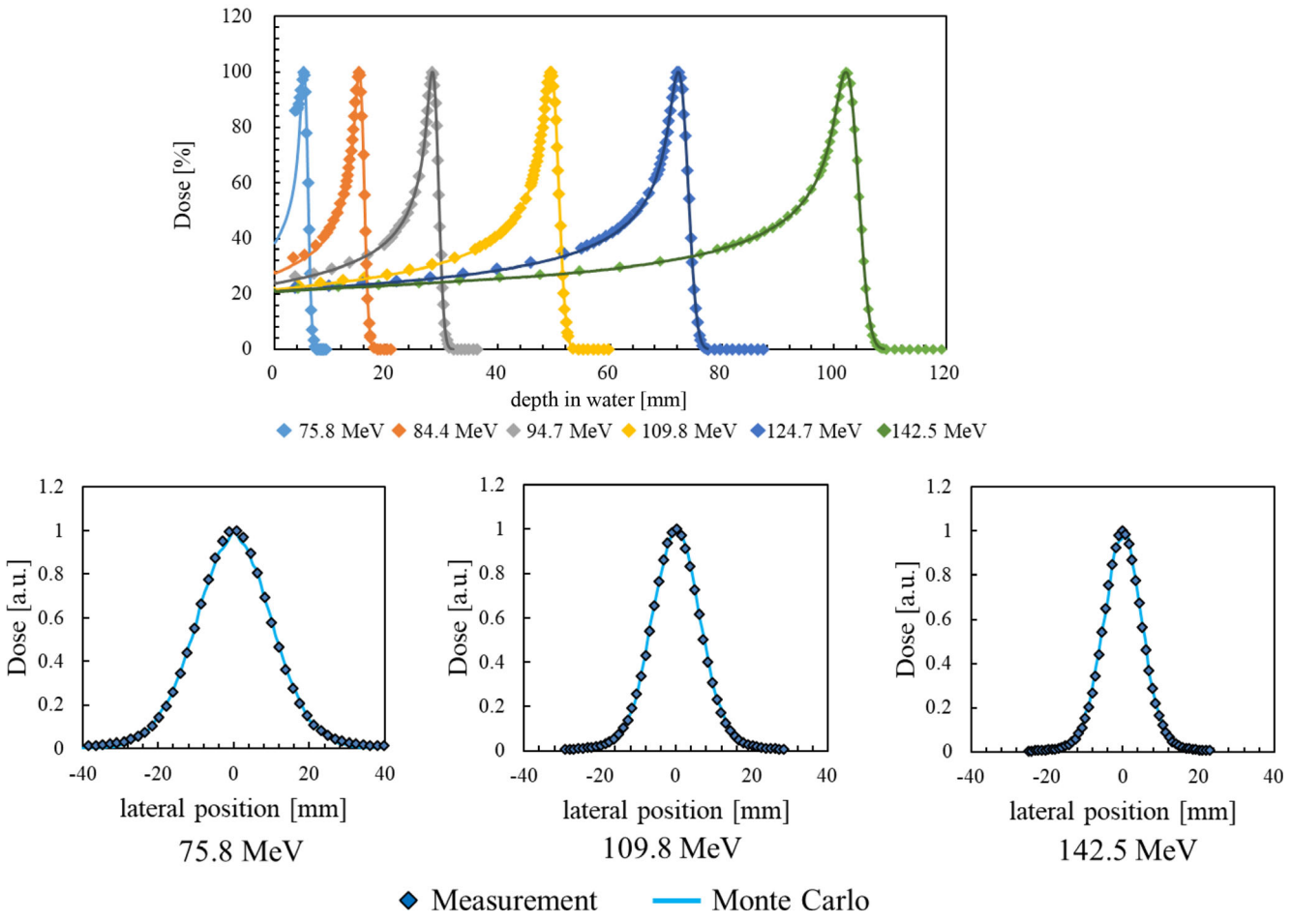

FIG. 2. Integral depth dose (upper row) and lateral profile at a 3-mm (for 75.8 MeV) and 5-mm (for 109.8 and 142.5 MeV) depth in water (lower row).

physical dose to the target was 2 Gy. The collimator opening size was set so to cover the edge of the proximal front of the targets with 50% of the prescribed dose.

2.B.3 | Physical dose and LET_d calculations

The physical dose and LET_d distributions were computed for collimator-scattered protons, unscattered protons, and both together. In the dose computation, the energy within each voxel was scored at each step for all particles and events, and the total sum was converted into the physical dose. In the LET_d computation, the primary, secondary, and higher order protons were included, while the hadrons, leptons, and neutral particles generated via nuclear reactions were excluded.[17] This was primarily because the estimated contributions of these other particles to the dose are much smaller than the protons (<1%), and they have large uncertainties for the dependence of biological parameters, that is, α and β, on LET_d.[17] For the computation of LET_d using Geant4, it has been discussed that the value changes among different scoring techniques, as well as the tracking step size limit.[18–20] In this study, we followed Cortés-Giraldo et al.[20] and used the following equation for computing LET_d:

$$LET_d = \frac{\sum_{n=1}^{N}\sum_{s=1}^{S_n} L_{sn}\varepsilon_{sn}}{\sum_{n=1}^{N}\sum_{s=1}^{S_n}\varepsilon_{sn}} \quad (1)$$

where n is the event index, S_n indicates the steps taken by the primary and secondary protons in the voxel for the n-th event, and ε_{sn} and L_{sn} are the energy deposited by proton and the mean energy loss per unit path length along the s-th step in the n-th event, respectively. To compute L_{sn}, the ComputeElectronicDEDX() function of the G4EmCalculator class was used.[15] From now on, the physical dose and LET_d originated from the collimator-scattered protons will be referred to as D^S and $= \pi r^2\ LET_d^S$, respectively, while those resulting from the unscattered protons and all protons (scattered + unscattered) will be indicated by the superscripts US and S + US, respectively.

2.C | RBE calculation

The RBE was calculated using the linear–quadratic (LQ)-based RBE model developed by McNamara et al.[22]:

$$RBE\left[D,\frac{\alpha}{\beta},LET_d\right] = \frac{1}{2D}\left(\sqrt{\left(\frac{\alpha}{\beta}\right)^2 + 4D\left(\frac{\alpha}{\beta}\right)RBE_{max} + 4RBE_{min}^2D^2} - \left(\frac{\alpha}{\beta}\right)\right) \quad (2)$$

where D is the physical dose, and α and β are the LQ parameters for the reference x-ray radiation. The LET_d dependence is implicit in RBE_{max} and RBE_{min}:

$$RBE_{max} = 0.99064 + \frac{0.35605}{(\alpha/\beta)}\ LET_d,$$
$$RBE_{min} = 1.1012 - 0.0038703 \times \sqrt{\frac{\alpha}{\beta}}\ LET_d.$$

2.D | Evaluation

The z-axis was the selected incident beam direction and its origin, $z = 0$, was located at the water surface; x and y were the transverse coordinates. We considered z_s = 5 mm as the representative normal tissue depth at the surface and z_c as the target center depth. The x-position receiving the maximum dose by the collimator-scattered protons at z_s was defined as x_s In this study, α/β was set to 10 Gy at the target center and to 3 Gy at z_s.[22] Note that these values fit for only some of the tumor sites. For the α/β parameter, a wide range of heterogeneity has been observed among tumor sites. In addition, recent literature review has revealed that the study heterogeneity for example, tumor stage, type of biological models and clinical endpoints gives large variation in the α/β parameter even for the same tumor site.[23]

The following parameters were evaluated for all the target geometries;

1. The maximum physical dose deposited by the collimator-scattered protons at the depth z_s along the x-axis, $D^S(x_s,0,z_s)$, and at the center of the target, $D^S(0,0,z_c)$, are both normalized by the D^{US} at the target center.
2. The dose-averaged LET for the collimator-scattered, unscattered, and all protons at $(x_s,0,z_s)$, that is, LET_d^S $(x_s,0,z_s)$, LET_d^{US} $(x_s,0,z_s)$, and LET_d^{S+US} $(x_s,0,z_s)$, and at the target center, that is, LET_d^S $(0,0,z_c)$, LET_d^{US} $(0,0,z_c)$, and LET_d^{S+US} $(0,0,z_c)$.
3. The relative biological effectiveness of the unscattered and all protons at $(x_s,0,z_s)$, that is, RBE^{US} $(x_s,0,z_s)$ and $RBE^{S+US}(x_s,0,z_s)$, and at the target center, that is, $RBE^{US}(0,0,z_c)$ and $RBE^{S+US}(0,0,z_c)$.

2.E | Patient treatment plan

Two simulated cases (Case A: ocular melanoma, Case B: childhood rhabdomyosarcoma) for which the collimator is beneficial to spare the surrounding normal organs were considered (Fig. 3). The

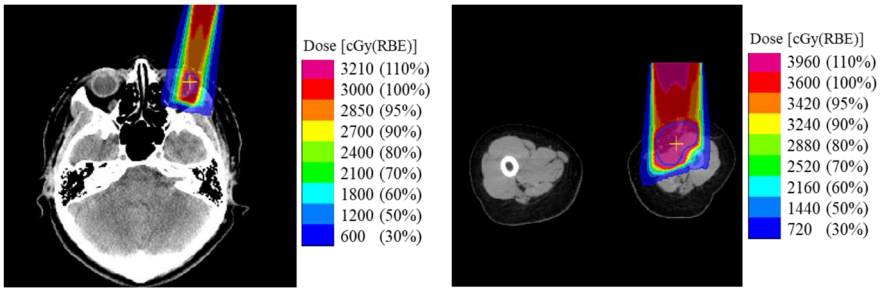

FIG. 3. Dose distributions for Cases A, ocular melanoma, (left) and B, childhood rhabdomyosarcoma, (right).

treatment plan was created with the VQA TPS (Hitachi Ltd., Tokyo). A pencil beam algorithm, in which the lateral fluence profile is modeled as a double-Gaussian function,[24,25] was used. The spot decomposition method was used to account for tissue heterogeneity and the collimator boundary across the beam's cross-section.[26,27] The prescriptions were given to D99 and D50 of the clinical target volume (CTV), respectively, assuming that the *RBE* had a constant value of 1.1. The CTV size, range and FS of the targets, and the prescription per field are summarized in Table 2. The single field was used in both plans, and a 5-mm collimator margin was selected to cover the CTV with the prescribed dose.

We evaluated the maximum dose increase nearby normal organs at the surface (lens in Case A and skin in Case B), the physical dose increase at the isocenter (set to the geometrical center of CTV), and the increases in LET_d and *RBE*. For Case B, the increase in RBE for the CTV was evaluated using α/β of 10 as well as 3 Gy following Mendonca et al.[28]

TABLE 2 Target geometry parameters and prescribed dose

Case	CTV size [ml]	Range [cm WEL]	Maximum SOBP width [cm WEL]	Field size (FS) [cm^2]	Prescribed dose/fraction [Gy(*RBE*)]
A	12	2.4	2	1.3 × 1.5	6 (30/5)
B	139	5.0	4.5	4.4 × 11.8	1.8 (36/20)

CTV = clinical target volume, WEL = water equivalent length, SOBP = spread-out Bragg peak

Note: The target FS was represented by the bounding rectangle of the target projected along the beam direction.

3 | RESULTS

3.A | Physical dose and LET_d distributions

Figures 4(a)–4(c) show the physical dose distributions in the *x*–*z* plane for unscattered, collimator-scattered, and all protons for target R15_S5_FS8. Along the collimator edge, clear lines of the scattered dose can be observed: they exhibit the largest value at the surface and monotonically decrease with depth.

The LET_d distributions are shown, for the same categorized protons, in Figs. 4(d)–4(f); LET_d^S exhibits larger values than LET_d^{US} at the same location in water. At the water surface, the LET_d^{US} distribution is nearly uniform along the *x*-direction in field and slightly increases toward the out-of-field region, while the LET_d^S one reaches its largest value (~8 keV/μm) at the field center, decreases to a quarter of it (~2 keV/μm) at the field boundary, and increases again toward the out-of-field region.

Figure 5 shows the D^S distribution at a 5-mm depth ($z = z_s$) along the *x*-axis for the targets R10_S10_FS16 (a) and R10_S10_FS2 (b), together with those of D^{US} and D^{S+US} for reference. Clear peaks can be observed at the collimator edge [Fig. 5(a)] but, as the FS is reduced, they overlap until they form a single large peak at the field center [Fig. 5(b)].

3.B | Physical dose increase

Figure 6(a) shows the maximum values of the scattered dose at a 5-mm depth ($z = z_s$) along the *x*-axis for the various target geometries listed in Table 1. The maximum dose increase ranges from 3 to 22%

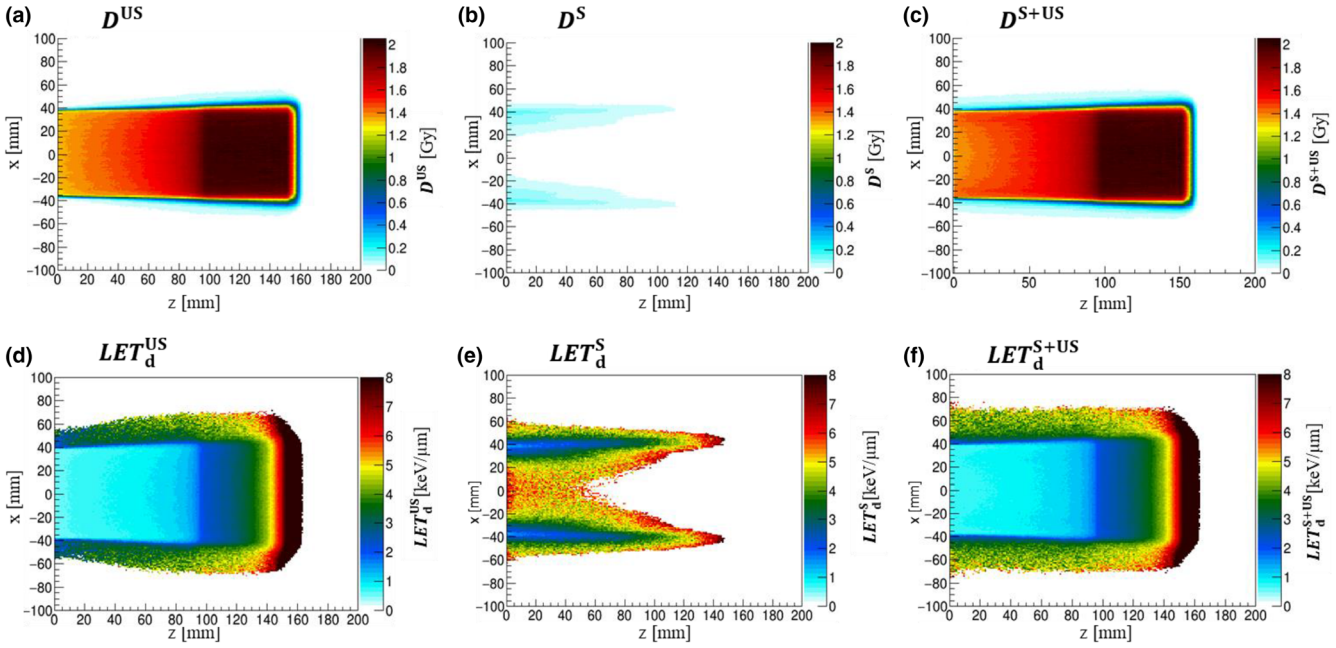

FIG. 4. Distributions of the physical dose (*D*) and dose-averaged linear energy transfer (LET_d) in the *x*-*z* plane, including the beam central axis for the target R15_S5_FS8, for the unscattered (superscript US), collimator-scattered (superscript S), and all (superscript S + US) protons. The displayed regions are restricted to voxels with $D^S > 0.01$ Gy.

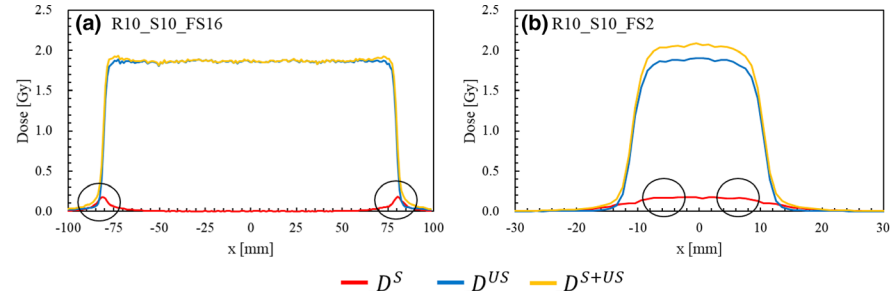

FIG. 5. Distributions of the physical dose from the collimator-scattered (D^S), unscattered (D^{US}), and all protons (D^{S+US}) at a 5-mm depth along the *x*-axis for the targets R10_S10_FS16 (a) and R10_S10_FS2 (b). The circled points indicate the *x*-positions receiving the maximum dose by the scattered protons.

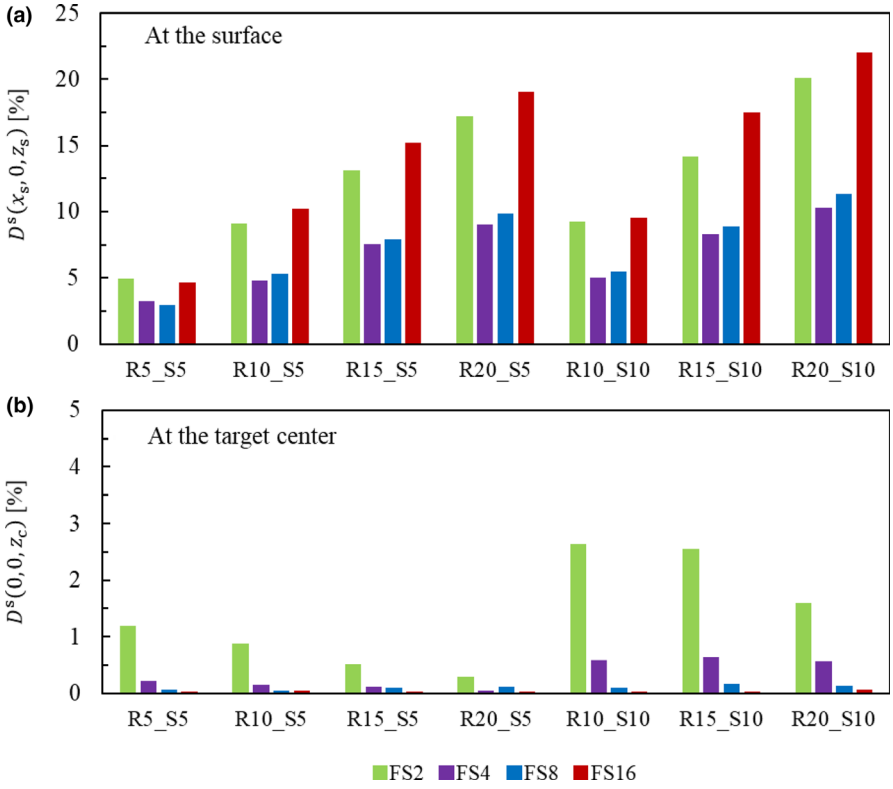

FIG. 6. Maximum values of the physical dose from the collimator-scattered protons (D^S) at a 5-mm depth along the *x*-axis (a) and at the target center (b), for the various target geometries listed in Table 1, normalized by the physical dose from the unscattered protons at the target center.

over all tested conditions. The dosimetric impact increases with the range; it also increases with SOBP for ranges of 15 and 20 cm but remains almost unchanged for the 10 cm. The FS dependence is not monotonous; that is, at small and large FSs, the dose increase is larger compared to that at middle-sized fields (FS = 4, 8) because, with a small FS, the overlapping scattered protons from several walls form the large central peak [see Fig. 5(b)]. In contrast, with a large FS, the beam angle with respect to the collimator wall increases, and so does the collimator scattering [see Fig. 5(a)]. The combination of these two effects results in the concave behavior against FS.

At the target center, the maximum scattered dose does not exceed 2.6% over all tested conditions, as shown in Fig. 6(b). It is largest with a small FS because of the largest overlap from the four collimator walls; for small FSs, the scatter dose decreases with the range because the scattered protons stop before reaching the target center.

3.C | LET_d increase

Figure 7(a) shows the LET_d^S, LET_d^{US}, and LET_d^{S+US} at a 5-mm depth ($z = z_s$) and at the *x*-position receiving the maximum scattered dose from the collimator. As expected, the relationship $LET_d^S > LET_d^{S+US} > LET_d^{US}$ holds in all tested targets, reflecting the protons' energy loss during scattering. However, although LET_d^S can reach values 6.6 times greater than the maximum LET_d^{US} at most, it does not largely influence the LET after the dose averaging: the maximum difference between LET_d^{S+US} and LET_d^{US} is 0.4 keV/μm.

Figure 7(b) shows the same quantities as Fig. 7(a) at the target centers. In this case, the collimator-scattered dose is as small as shown in Fig. 6(b) (2.6% at most). Hence, even if LET_d^S can reach large values as 14.3 keV/μm (target R10_S10_FS16), LET_d^{S+US} and LET_d^{US} are almost equal in all tested conditions (with a maximum difference of 0.08 keV/μm). In addition, both LET_d^{S+US} and LET_d^{US} are almost constant against the FS.

3.D | RBE increase

Figure 8(a) compares the RBE^{US} and RBE^{S+US} at a 5-mm depth ($z = z_s$) and at the *x*-position receiving the maximum scattered dose from the collimator. Due to the increase in the LET_d^S (see Fig. 7), RBE^{S+US} is always greater than RBE^{US}; however, the

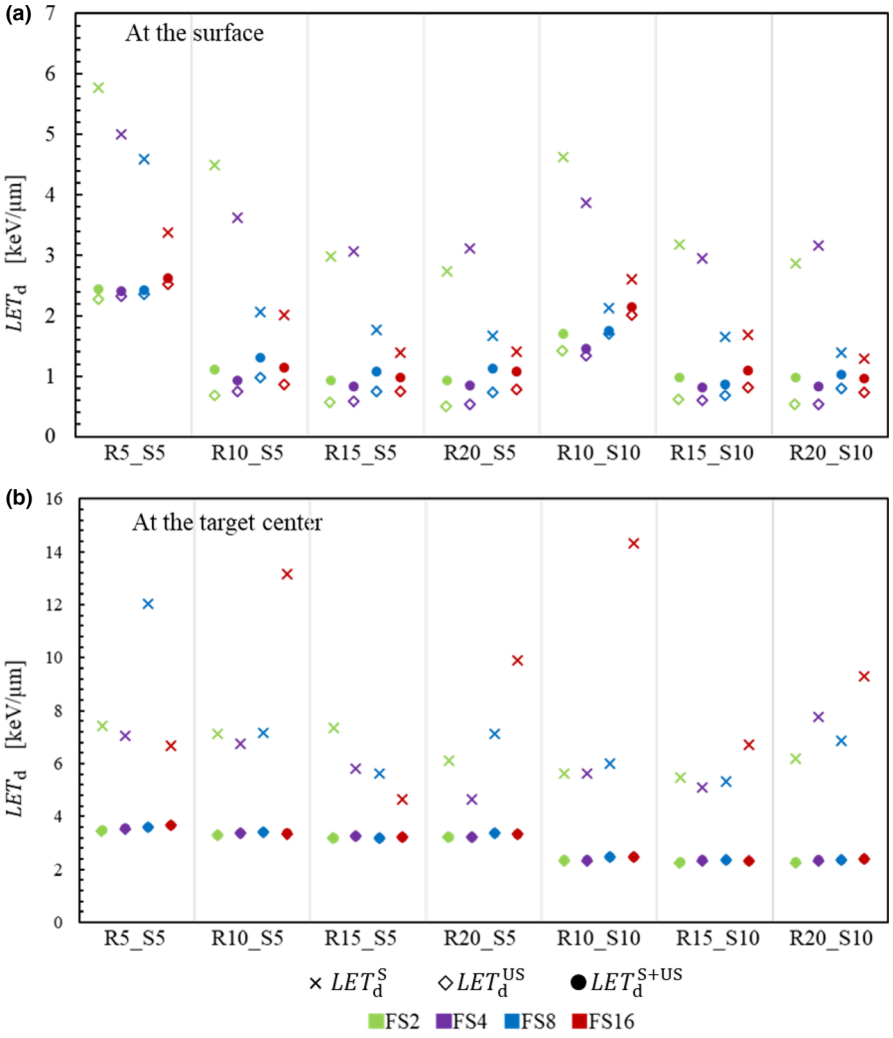

FIG. 7. Dose-averaged linear energy transfer from collimator-scattered (LET_d^S), unscattered (LET_d^{US}), and all protons (LET_d^{S+US}) at a 5-mm depth and at the x-position receiving the maximum scattered dose from the collimator (a) and at the target center (b) for the various target geometries listed in Table 2.

magnitude of *RBE* increase is not significant because its maximum is only 0.04.

Figure 8(b) compares the same quantities at the target center. In this case, since LET_d does not change when the collimator-scattered protons are included (see Fig. 7), the change in *RBE* is negligible.

3.E | Physical dose, LET_d, and RBE increase with the patient geometry

Table 3 shows the simulation results for the patient plans. The dose increase rate by the collimator scattering is described in terms of D^{US} at the isocenter (5.5 Gy for Case A and 1.7 Gy for Case B). The closest target geometry of Case A among our tested conditions is R5_S5_FS2; the scattered dose is about 2.4% (Case A) and 5% (target R5_S5_FS2) at the surface. The patient plan has smaller scatter dose compared to the tested geometry mainly because both the range and SOBP are approximately 2 cm, which is smaller than the tested conditions. On the other hand, the Case B geometry is considered located between the targets R5_S5_FS4 and R5_S5_FS8. The water phantom simulation indicates a dose increase of about 3%, while a 4.2% increase is observed in Case B; this dose enhancement in patient geometry may be due to the overlap of the scattered doses from the sharp corners of the collimator and the skin location. The skin starts from the zero depth, where the scattered dose is maximum.

With regard to the LET_d and *RBE* increase, the changes from LET_d^{US} to LET_d^{S+US} and from RBE^{US} to RBE^{S+US} were calculated. The evaluation was done at the maximum dose point in the lens, for Case A, and skin, for Case B. In Case A, since the scattered dose is small, the LET_d increase is about 2.0% and the *RBE* does not increase at all; this result is slightly different from that of the target R5_S5_FS2, where the LET_d and *RBE* increase are 7.7% and 0.5%, respectively. As mentioned above, this difference is accounted for by the difference in range between the targets. In Case B, LET_d and *RBE* increase by 8.2% and 0.9%, respectively, while, in the targets R5_S5_FS4 and R5_S5_FS8, their increases are 2.8%–3.8% and 0.1%–0.2%, correspondingly. This difference may be attributed to the slight difference in the evaluation depth, as mentioned above. In both cases, we can observe a negligible increase in *RBE*, as expected from the simulations with test geometries.

For the target isocenter, the physical dose increase was 1.5% and less than 0.1% for Case A and B, respectively. No increase in

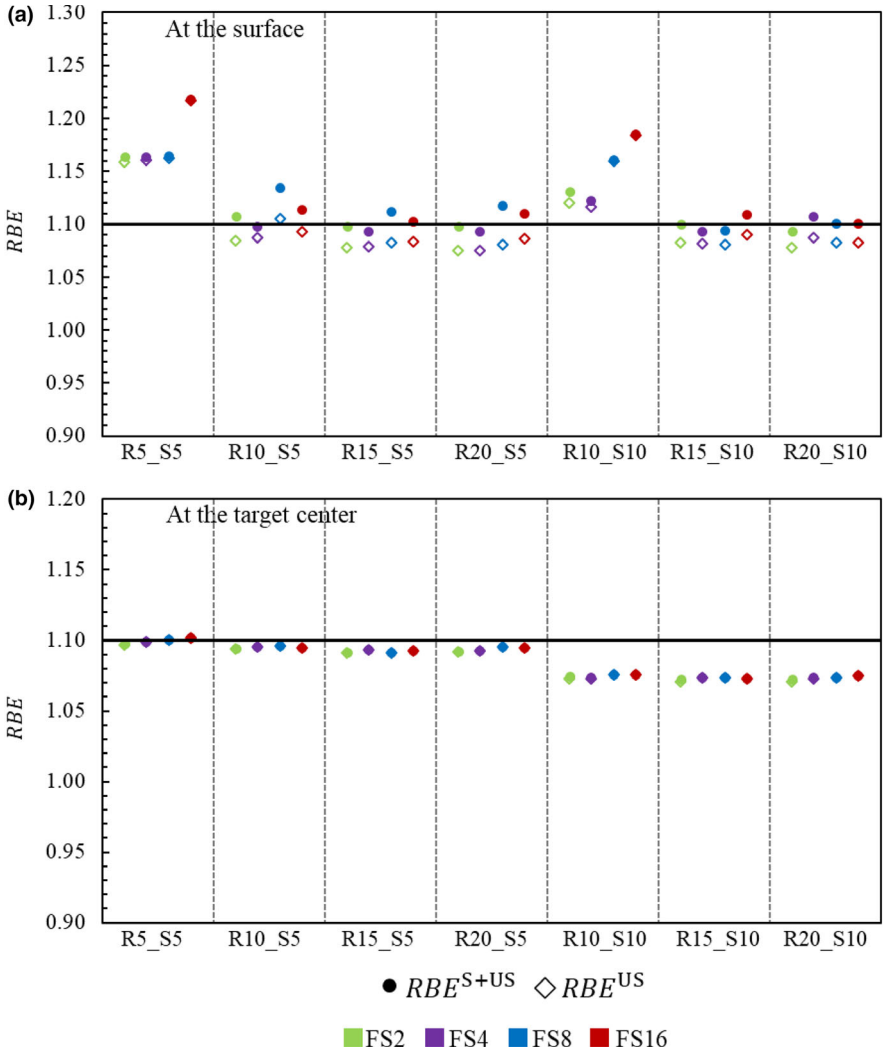

FIG. 8. Relative biological effectiveness from the unscattered (RBE^{US}) and the scattered + unscattered protons (RBE^{S+US}) for the various target geometries listed in Table 2, at a 5-mm depth, and at the *x*-position receiving the maximum dose (α/β = 3 Gy) (a) and at the target center (α/β = 10 Gy) (b).

RBE was observed in both cases, regardless of the α/β values (10 and 3 Gy).

4 | DISCUSSION

We investigated the physical and biological impacts of collimator-scattered protons used in a PBS system. In their pioneering work, van Luijk et al.[6] focused on very small field sizes (up to 2 × 2 cm^2), while this work was a systematic survey of FS up to 16 × 16 cm^2, which covers a wider range of tumor sites and is almost the same size as that investigated by Titt et al.[7] In the passive scattering, the impact of collimator scattering rapidly decreases as the FS increases from 3 × 3 to 10 × 10 cm^2 and does not change from 10 × 10 to 15 × 15 cm^2 (see Fig. 4 in Titt et al.[7]). We found that, in contrast to the passive scattering, the impact becomes large not only at small, but also large FSs, and this was attributed to the difference in proton beams' directionality between PBS and passive scattering. In passive scattering, the beam angle has a little correlation with the distance from the beam axis but, in PBS, the beam has a finite angle that is proportional to the lateral displacement with respect to the beam central axis. Since the X and Y scanning magnets are placed at different positions, the impact size is different among the scanned directions. Aside from the FS dependence, the physical dose impact by collimator-scattered protons observed in this research is consistent (or, at least, is not in contrast) with the research of Titt et al.[7] In both studies, the physical dose impact increases with the range at the water surface, according to the increased number of protons passing through the collimator; at the target center, the impact is comparable between different ranges and weakly increases with SOBP.

To the best of our knowledge, this is the first study of the biological impact of collimator-scattered protons using the LQ-based LET-dependent *RBE* model. In both water surface and target center depth, the LET_d^S is highest at the field center and can exceed 10 keV/μm. However, the scatter dose is not large enough to increase the total LET_d by 1.0 keV/μm. Although we have reported results for only limited positions in each geometry, this is true for all the positions and geometries receiving a dose >0.3 Gy (15% of that at the target center). Figure 9 shows the scatter plot for the LET_d

TABLE 3 The increases in physical dose (D^S), LET_d, and *RBE* by the collimator scattering in OAR. LET_d and *RBE* were evaluated at the maximum D^S point in OAR

Case	Maximum D^S in OAR [Gy]	Maximum D^S rate in OAR [%]	LET_d increase rate [%]	*RBE* increase rate [%]
A	0.13 (lens)	2.4	2.0	0.0
B	0.07 (skin)	4.2	8.2	0.9

OAR = organ at risk, LET_d = dose-averaged linear energy transfer, RBE = relative biological effectiveness.

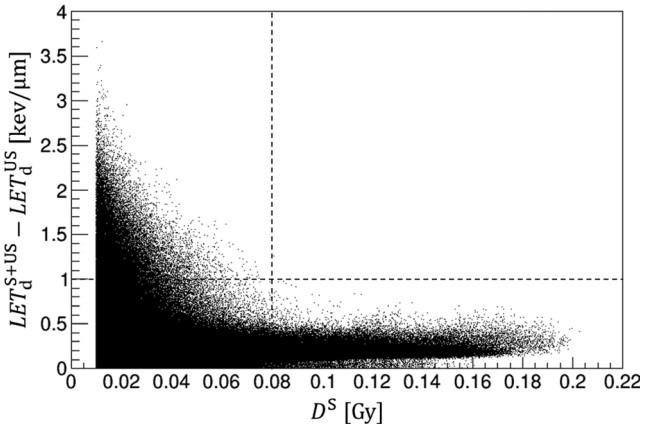

FIG. 9. The increase in dose-averaged linear energy transfer (LET_d) against the increases in physical dose from the collimator-scattered protons (D^S) for the target R15_FS8_S5, based on the voxels receiving more than 0.01 Gy.

increase ($LET_d^{S+US} - LET_d^{US}$) against the D^S increase for the target R15_FS8_S5: all the voxels receiving a D^S above 0.01 Gy are plotted. In general, an LET_d increase greater than 1 keV/μm is observed only in the voxels receiving small D^S (<0.08 Gy, that is, 4% dose of the prescription); in those receiving a large D^S (>0.08 Gy), instead, there is only a small increase (<1 keV/μm). This indicates that the enhanced LET_d^S does not affect the total LET_d, not only at the water surface and target center depth but at all positions.

One of the limitations of this work is that the number of scattered protons at the target center was not large enough to have statistically meaningful results. The large LET_d^S variations observed for several geometries in Fig. 7 at FS $\geq 8 \times 8$ cm^2 may be due to the statistical uncertainty. However, the input values for the *RBE* model (LET_d^{S+US} and LET_d^{US}) were both calculated with a sufficient number of protons and gave reliable estimations.

We used the LQ-based *RBE* model developed by McNamara et al.[21] Due to the large variation in the *RBE* estimates because of the fundamental differences in experimental databases, model assumptions, and regression techniques,[29] we estimated the model dependence of our results using two other models.[30,31] Different *RBE* models give different *RBE*; however, in both models, the magnitude of *RBE* increase is not significant (lower than 0.03 and 0.06 at the water surface and 0.003 and 0.005 at the target center, respectively).

The patient plan simulation results are almost consistent with the rectangular targets in the water phantom. However, due to the large variations of collimator shape and OAR location, the physical dose increase must be assessed patient-by-patient. Several analytical approaches have been proposed for passive scattering in the past[28,32,33] to account for the collimator-scattered protons in the TPS dose calculation engine. Several versions of fast Monte Carlo simulations[34] have recently become available in commercial TPS, making it possible to evaluate the physical dose impact of collimator scattering in minutes with accuracy. Such simulation tools could enhance the PBS accuracy when using a collimator. On the other hand, when calculating LET_d and *RBE*, the scattered dose contribution can be neglected; analytical LET_d and *RBE* calculations[35,36] are promising methods for this purpose.

In this study, a patient-specific collimator was used to effectively create a sharp penumbra along the outermost contour of the target. As an alternative, apertures that can adapt their shapes energy layer-by-energy layer have been developed,[2,4] but they may suffer from a greater collimator scattering in return for the increased conformity, which could be the subject of future investigations.

5 | CONCLUSIONS

Both the physical and biological impacts of the collimator-scattered protons used in PBS proton therapy were studied. Monte Carlo simulations revealed that a non-negligible amount of physical dose was contaminated by the collimator scattering (3.0%–22.0% at the surface). The observed behavior was similar (or, at least, not contradictory) to previous research about the range and SOBP dependence in passive scattering. On the other hand, a different behavior was observed in terms of FS between PBS and passive scattering. The collimator-scattered protons exhibited LET_d up to 6.6 times greater than the unscattered ones. However, when averaged by dose, the total LET_d was barely increased compared to the unscattered protons. Therefore, increased biological impact by the collimator-scattered protons can be almost entirely attributed to an increased physical dose and not to the increase in RBE due to the LET_d increase.

ACKNOWLEDGMENTS

We wish to thank Dr. Takaaki Fujii, Mr. Tetsuhiro Sodeta, and Mr. Yu Hiyama for their valuable support. This research was supported by JSPS KAKENHI Grant No. 18K07621 and the "Global Institution for Collaborative Research and Education (GI-CoRE), Hokkaido University", founded by the Ministry of Education, Culture, Sports, Science and Technology (MEXT), Japan.

CONFLICT OF INTERESTS

We disclose that Shusuke Hirayama received funds from Hitachi, Ltd., Tokyo, Japan.

REFERENCES

1. Safai S, Bortfeld T, Engelsman M, et al. Comparison between the lateral penumbra of a collimated double-scattered beam and uncollimated scanning beam in proton radiotherapy. *Phys Med Biol*. 2008;53:1729–50.
2. Hyer DE, Hill PM, Wang D, et al. A dynamic collimation system for penumbra reduction in spot-scanning proton therapy: proof of concept. *Med Phys*. 2014;41:091701.
3. Yasui K, Toshito T, Omachi C, et al. A patient-specific aperture system with an energy absorber for spot scanning proton beams: verification for clinical application. *Med Phys*. 2015;42:6999–7010.
4. Langenegger A, Huang K, Rosenthal S, Cooley J. 2018 The advantage of multi-layer shaping using the Mevion Adaptive. Aperture PTCOG, 57th; 2018.
5. Moteabbed M, Yock TI, Depauw N, et al. Impact of spot size and beam-shaping devices on the treatment plan quality for pencil beam scanning proton therapy. *Int J Radiat Oncol Biol Phys*. 2016;95:190–198.
6. Yasui K, Toshito T, Omachi C, et al. Evaluation of dosimetric advantages of using patient specific aperture system with intensity modulated proton therapy for the shallow depth tumor. *J Appl Clin Med Phys*. 2018;19:132–137.
7. van Luijk P, van't Veld AA, Zelle HD, et al. Collimator scatter and 2D dosimetry in small proton beams. *Phys Med Biol*. 2001;46:653–670.
8. Titt U, Zheng Y, Vassiliev ON, et al. Monte Carlo investigation of collimator scatter of proton-therapy beams produced using the passive scattering method. *Phys Med Biol*. 2007;53:487–504.
9. Paganetti H. Relative biological effectiveness (RBE) values for proton beam therapy. Variations as a function of biological endpoint, dose, and linear energy transfer. *Phys Med Biol*. 2014;59:R419–R472.
10. Matsumoto Y, Matsuura T, Wada M, Egashira Y, Nishio T, Furusawa Y. Enhanced radiobiological effects at the distal end of a clinical proton beam: in vitro study. *J Radiat Res*. 2014;55:816–822.
11. Guan F, Bronk L, Titt U, et al. Spatial mapping of the biologic effectiveness of scanned particle beams: towards biologically optimized particle therapy. *Sci Rep*. 2015;5:9850.
12. Howard ME, Beltran C, Anderson S, et al. Investigating dependencies of relative biological effectiveness for proton therapy in cancer cells. *Int J Part Ther*. 2018;4:12–22.
13. Michaelidesová A, Vachelová J, Puchalska M, et al. Relative biological effectiveness in a proton spread-out Bragg peak formed by pencil beam scanning mode. *Austr Phys Eng Sci Med*. 2017;40:359–368.
14. Peeler CR, Mirkovic D, Titt U, et al. Clinical evidence of variable proton biological effectiveness in pediatric patients treated for ependymoma. *Radiother Oncol*. 2016;121:395–401.
15. Giovannini G, Böhlen T, Cabal G, Bauer J, Tessonnier T, Frey K. Variable RBE in proton therapy: comparison of different model predictions and their influence on clinical-like scenarios. *Radiat Oncol*. 2016;11:1–16.
16. Agostinelli S, Allison J, Amako KA, et al. GEANT4—a simulation toolkit. *Nucl Instr Meth Phys Res Sect A*. 2003;506:250–303.
17. Aso T, Kimura A, Kameoka S, Murakami K, Sasaki T, Yamashita T. Geant4 based simulation framework for particle therapy system. *Nucl Sci Symp IEEE Conf Rec*. 2007;4:2564–2567.
18. Grassberger C, Paganetti H. Elevated LET components in clinical proton beams. *Phys Med Biol*. 2011;56:6677–6691.
19. Granville DA, Sawakuchi GO. Comparison of linear energy transfer scoring techniques in Monte Carlo simulations of proton beams. *Phys Med Biol*. 2015;60:N283.
20. Guan F, Peeler C, Bronk L, et al. Analysis of the track-and dose-averaged LET and LET spectra in proton therapy using the geant4 Monte Carlo code. *Med Phys*. 2015;42:6234–6247.
21. Cortés-Giraldo MA, Carabe A. A critical study of different Monte Carlo scoring methods of dose average linear-energy-transfer maps calculated in voxelized geometries irradiated with clinical proton beams. *Phys Med Biol*. 2015;60:2645–2669.
22. McNamara AL, Schuemann J, Paganetti H. A phenomenological relative biological effectiveness (RBE) model for proton therapy based on all published in vitro cell survival data. *Phys Med Biol*. 2014;60:8399–8416.
23. Williams MV, Denekamp J, Fowler JF. A review of $\alpha\beta$ ratios for experimental tumors: implications for clinical studies of altered fractionation. *Int J Radiat Oncol Biol Phys*. 1985;11:87–96.
24. van Leeuwen CM, Oei AL, Crezee J. The alfa and beta of tumours: a review of parameters of the linear-quadratic model, derived from clinical radiotherapy studies. *Radiat Oncol*. 2018;13:96.
25. Zhu XR, Poenisch F, Lii M, et al. Commissioning dose computation models for spot scanning proton beams in water for a commercially available treatment planning system. *Med Phys*. 2013;40:041723.
26. Hirayama S, Takayanagi T, Fujii Y, et al. Evaluation of the influence of double and triple Gaussian proton kernel models on accuracy of dose calculations for spot scanning technique. *Med Phys*. 2016;43:1437–1450.
27. Schaffner B, Pedroni E, Lomax A. Dose calculation models for proton treatment planning using a dynamic beam delivery system: an attempt to include heterogeneity effects in the analytical dose calculations. *Phys Med Biol*. 1999;44:27–41.
28. Slopsema R, Matysiak W. SU-F-T-145: modeling of a proton pencil beam partially blocked by a collimator. *Med Phys*. 2016;43:3495.
29. Mendonca M, Timmerman RD. In regard to Donaldson et al.: results from the IRS-IV randomized trial of hyperfractionated radiotherapy in children with rhabdomyosarcoma-a report from the IRSG. IJROBP 2001;51:718–728. *Int J Radiat Oncol Biol Phys*. 2002;54:1579–1580.
30. Rørvik E, Fjæra LF, Dahle TJ, et al. Exploration and application of phenomenological RBE models for proton therapy. *Phys Med Biol*. 2018;63:185013.
31. Wedenberg M, Toma-Dasu I. Disregarding RBE variation in treatment plan comparison may lead to bias in favor of proton plans. *Med Phys*. 2013;41:091706–091709.
32. Carabe A, España S, Grassberger C, Paganetti H. Clinical consequence of relative biological effectiveness variations in proton radiotherapy of the prostate, brain and liver. *Phys Med Biol*. 2013;58:2103–2117.
33. Vidal M, De Marzi L, Szymanowski H, et al. An empirical model for calculation of the collimator contamination dose in therapeutic proton beams. *Phys Med Biol*. 2016;61:1532–1545.
34. Matsinos E. Collimator effects in proton planning. arXiv preprint arXiv:0811.1076; 2008.
35. Fippel M, Soukup M. A Monte Carlo dose calculation algorithm for proton therapy. *Med Phys*. 2004;31:2263–2273.
36. Wilkens JJ, Oelfke U. Analytical linear energy transfer calculations for proton therapy. *Med Phys*. 2003;30:806–815.
37. Hirayama S, Matsuura T, Hideaki U, et al. An analytical dose-averaged LET-calculation algorithm considering the off-axis LET enhancement by secondary protons for spot-scanning proton therapy. *Med Phys*. 2018;45:3404–3416.

SUPPORTING INFORMATION

Additional supporting information may be found online in the Supporting Information section at the end of the article.

Fig S1. Depth dose profiles along the beam central axis (a-1, b-1) and lateral profiles at a 5-mm depth in water (a-2, b-2) for the targets R10_FS2_S10 (a-1, a-2) and R10_FS8_S10 (b-1, b-2), respectively.